TISSUE ENGINEERING: Part A
Volume 27, Numbers 1 and 2, 2021

DOI: 10.1089/ten.tea.2020.0005

termis
Tissue Engineering
& Regenerative Medicine
International Society

ORIGINAL ARTICLE

Bioengineered Skeletal Muscle as a Model of Muscle Aging and Regeneration

Nika Rajabian, MS,[1] Aref Shahini, MS,[1] Mohammadnabi Asmani, PhD,[2] Kalyan Vydiam, MS,[2] Debanik Choudhury, MS,[1] Thy Nguyen, BC,[2] Izuagie Ikhapoh, PhD,[1] Ruogang Zhao, PhD,[2] Pedro Lei, PhD,[1] and Stelios T. Andreadis, PhD[1–3]

With age, adult skeletal muscle (SkM) is known to decrease in muscle mass, strength, and functional capacity, a state known as sarcopenia. Here we developed an *in vitro* three-dimensional (3D) bioengineered senescent SkM tissue using primary human myoblasts. These tissues exhibited the characteristics of atrophied muscle, including expression of senescent genes, decreased number of satellite cells, reduced number and size of myofibers, and compromised metabolism and calcium flux. As a result, senescent SkM tissues showed impaired ability to generate force in response to electrical stimulation compared with young tissues. Furthermore, in contrast to young SkM tissues, senescent tissues failed to regenerate in response to injury, possibly as a result of persistent apoptosis and failure to initiate a proliferation program. Our findings suggest that 3D senescent SkM may provide a powerful model for studying aging and a platform for drug testing and discovery of therapeutic compounds to improve the function of sarcopenic muscle.

Keywords: bioengineered muscle, human skeletal muscle, senescence, contractility, muscle regeneration

Impact Statement

Skeletal muscle (SkM) plays important physiological roles and has significant regenerative capacity. However, aged SkM lose their functionality and regeneration ability. In this article, we present a senescent human bioengineering SkM tissue model that can be used to investigate senescence, metabolic or genetic diseases that inflict SkM, and to test various strategies including novel small molecules that restore muscle function and promote regeneration. One key limitation of two-dimensional cell culture system is the detachment of contractile myotubes from the surface over time, thereby limiting the evaluation of myogenic function. Here we use primary human myoblasts, which exhibit all major hallmarks of aging to mimic the organization and function of native muscle. Using this system, we were able to measure the contractile function, calcium transients, and regeneration capacity of SkM tissues. We also evaluated the response of senescent SkM tissues to injury and their ability to regenerate and recover, compared with ''young'' tissues. Our results suggest that three-dimensional constructs enable organization of contractile units including myosin and actin filaments, thereby providing a powerful platform for the quantitative assessment of muscle myotubes in response to injury, genetic or metabolic disorders, or pharmacological testing.

Introduction

Skeletal muscle (SkM) comprises 45–55% of body mass and plays essential physiological roles in the body such as enabling skeletal movements and regulating metabolism. However, aging leads to a significant decrease in SkM mass, strength, and metabolic performance,[1–3] compromising muscle stem cell function and regenerative capacity.[4] This decline in muscle mass and function is termed sarcopenia and often results in frailty and physical disability, increasing the incidences of injury, for example, falls and having adverse effects on the quality of life of the elderly people. As a result, the requirements for help with daily functions (e.g., bathing, dressing, household chores, and transportation) may also increase, ultimately leading to increased health care costs, estimated to be $\sim$18 billion dollars annually.[5]

Departments of [1]Chemical and Biological Engineering and [2]Biomedical Engineering, University at Buffalo, The State University of New York, Buffalo, New York, USA.
[3]Center of Excellence in Bioinformatics and Life Sciences, Buffalo, New York, USA.

SkM regeneration relies on the ability of myogenic progenitors to proliferate and fuse into multinucleated myofibers.[6] With aging, these cells lose their proliferation and differentiation potential, and SkM tissues exhibit decreased fiber number, volume, and contractile protein content, and dysregulated calcium flux, leading to significantly impaired contractile force generation.[7] Consequently, senescent SkM develops sarcopenia and fails to regenerate efficiently in response to injury.

In this study, we developed a three-dimensional (3D) model of senescent SkM tissue to examine the consequences of senescence on the physiological function and regenerative potential. Although previous studies have reported the development of a 3D *in vitro* SkM aging model, they made use of a mouse myoblast cell line, C2C12 (a subclone of C2 myoblasts),[8,9] thereby raising concerns as to whether cells that proliferate indefinitely can faithfully reproduce all aspects of aging, given that they do not exhibit well-accepted hallmarks of cellular senescence such as decreased proliferation rate, expression of senescence associated beta-galactosidase (SA-β-Gal), and DNA damage. In our study, we used primary human myoblasts that were subjected to >20 population doublings (equivalent to >50 days of culture) to develop tissues that exhibited all major hallmarks of senescence including expression of senescence-associated genes/proteins, significantly decreased proliferation, and impaired ability to form myotubes. In turn, our SkM tissue constructs engineered with senescent cells exhibited the hallmarks of senescent SkM, such as fewer and smaller myofibers, reduced contractile protein content, dysregulated calcium release, and compromised muscle energetics and mitochondrial function. Ultimately, senescent tissues exhibited significantly reduced ability to generate contractile force and regenerate in response to injury, similar to SkM tissue from aged individuals. Therefore, senescent bioengineered SkM may present a powerful model to study aging and a platform for genetic or pharmacological testing to facilitate drug discoveries to ameliorate sarcopenia, restore muscle function, and combat frailty.

Materials and Methods

Cell culture

Human myoblasts were obtained from Cook MyoSite (Pittsburgh, PA). Cells were isolated from quadriceps muscle of three donors (25-year-old woman, 68-year-old man, and 75-year-old woman). The cells were seeded at 3×10^3 cell/cm^2 in Matrigel (0.1 mg/ml) (CORNING, Corning, NY)-coated T175 flasks and cultured in SkM cell growth medium (GM)[10–12] composed of high glucose Dulbecco's modified Eagle's medium (DMEM; Gibco, Grand Island, NY), basic fibroblast growth factor (1 ng/mL), insulin (10 μg/mL), epidermal growth factor (10 ng/mL), dexamethasone (0.4 μg/mL), fetuin (50 μg/mL), bovine serum albumin (BSA; 500 μg/mL), gentamicin (50 μg/mL), and supplemented with 20% fetal bovine serum (FBS; Atlanta Biologicals, Flowery Branch, GA). The cells were cultured in a humidified incubator at 37°C and 10% CO_2 and the medium was replenished every other day. Cells were passaged every 4–5 days before they reached 80% confluence.

To differentiate myoblasts into multinucleated myotubes, myoblasts were seeded on Matrigel (0.1 mg/mL)-coated dishes and allowed to reach >90% confluence in GM. Then the cells were switched to differentiation medium (DM) composed of high-glucose DMEM supplemented with insulin (10 μg/mL), epidermal growth factor (10 ng/mL), BSA (500 μg/mL), and gentamicin (50 μg/mL) for a period of 7 days.

Adenosine triphosphate and lactate measurement assay

Myoblasts were seeded on Matrigel (0.1 mg/ml)-coated 48-well plates (60×10^3 cell/cm^2) and allowed to reach >90% confluence in GM. Then the cells were switched to DM for 7 days before the intracellular adenosine triphosphate (ATP) and extracellular lactate were measured. ATP concentration was measured per manufacturer's instructions. In brief, 50 μL of detergent was added to each sample for 5 min to lyse the cells under continuous mixing in an orbital shaker at 600–700 rpm. Fifty microliters of substrate solution was then added to cell lysate and incubated for 5 min in an orbital shaker at 600–700 rpm. Fifty microliters of each lysate was transferred to a well in a 96-well plate and luminescence was recorded using a Biotek Synergy 4 plate reader as directed by the manufacturer (background luminescence of empty wells was subtracted from each value).

For lactate measurements, 50 μL medium was collected from each sample of differentiated cells and transferred to 96-well plates. Lactate Detection Reagent (Promega, Madison, WI) (50 μL per well) was added to each sample and shaken for 30–60 s in an orbital shaker. After 60 min of incubation at room temperature (RT), luminescence was recorded as described previously.

Measurements of cell diameter and volume

To measure the cell diameter and volume, cells were detached from the surface by trypsin and resuspended in phosphate-buffered saline (PBS). Then 10 μL of the cell suspension was transferred onto a glass slide for imaging. Cells were imaged using a Zeiss Axio Observer Z1 (LSM 510; Zeiss, Oberkochen, Germany) microscope and a 10× objective (Plan-APOCHROMAT), and cell size was measured using ImageJ software.

Measurements of total protein content

Cells grown on tissue culture plates were lysed using lysis buffer [(62.5 mM Tris-HCl, pH 6.8 at 25°C), 2% (w/v) sodium dodecyl sulfate (SDS), 10% (v/v) glycerol, 0.1% (w/v) bromophenol blue, supplemented with 41.67 mM dithiothreitol] (Cell Signaling Technology, Danver, MA), supplemented with protease inhibitor cocktail (Sigma-Aldrich, St. Louis, MO), and the protein concentration was measured using the Bradford assay.[13]

Senescence-associated-β-galactosidase

The SA-β-Gal activity was detected using the β-Gal Staining Kit (Invitrogen) according to the manufacturer's instructions except that citric acid/sodium phosphate-buffered staining solution (pH 6.0) was used as described previously.[14] Cells were photographed using the Zeiss Axio Observer Z1a microscope and a 10× objective (Plan-APOCHROMAT). The number of SA-β-Gal-positive and total cells were counted in five randomly selected fields of view (total of >250 cells were counted per sample).

Immunocytochemistry

Myoblasts were fixed in 10% formalin for 10 min at RT. The fixed cells were permeabilized with 0.1% (v/v) Triton X-100/PBS for 10 min at RT and blocked with blocking buffer [5% (v/v) goat serum in 0.01% (w/v) Triton X-100/PBS] at RT for 1 h. Next, samples were immunostained with antibodies against myosin heavy chain (MYHC; Clone No. A4.1025, 1:500 dilution in blocking buffer; Millipore, Billerica, MA), sarcomeric alpha actinin (SAA; Clone No. EP2529Y, 1:200 dilution in blocking buffer; Abcam), γH2AX (Clone No. S139, 1:200 in blocking buffer; Cell Signaling Technology), H3K9me3 (Cat No. ab8898, 1:500 in blocking buffer; Abcam), H3K27me3 (Clone No. C36B11, 1:200 in blocking buffer; Cell Signaling Technology), desmin (Clone No. D93F5, 1:100 in blocking buffer; Cell Signaling Technology), and TE7 (Clone No. CBL271, 1:200 in blocking buffer; Millipore). Subsequently, the cells were stained with Alexa Fluor 594 or 488 conjugated goat anti-mouse or goat anti-rabbit antibodies (1:200 dilution in blocking buffer; ThermoFisher Scientific) and counterstained with Hoechst 33342 nuclear dye for 5 min (1:400 dilution in PBS; ThermoFisher Scientific).

Live/dead staining was carried out using the LIVE/DEAD® Viability/Cytotoxicity Kit, according to the manufacturer's protocol (ThermoFisher Scientific). Mitotracker staining was carried out using Red CMXRos (ThermoFisher Scientific) following the manufacturer's protocol. Images of cells were acquired using Zeiss Axio Observer Z1 (LSM 510; Zeiss, Oberkochen, Germany) equipped with digital camera (ORCA-ER C4742-80; Hamamatsu, Bridgewater, NJ).

Skeletal muscle microtissues

Micropost arrays containing 13 × 6 microwells (length: 800 μm; height: 227 μm; Fig. 2E), each containing two micropillars with heads, were prepared with polydimethylsiloxane (PDMS; Sylgard 184; Dow-Corning, Midland, MI) as described previously.[15] Next, the myoblasts (5×10^5 cells per device) were mixed with 1 mg/mL rat tail collagen type I (Corning®; Riverfront Plaza, NY) containing 20% (v/v) Matrigel at 4°C. This mixture was neutralized by 1 M NaOH, and immediately seeded on the devices. The microtissues formed between the two pillars were cultured in GM for 2 days followed by 7 days in DM. Senescent microtissues were prepared with cells that underwent replicative senescence in two-dimensional (2D) culture.

Bioengineered human muscle bundle

Human myobundles were prepared as described previously.[16] Specifically, 3D printed tissue molds were fabricated from polylactic acid at the University at Buffalo Digital Manufacturing Lab (length: 28 mm; width: 18 mm; height: 4 mm, Supplementary Fig. S4A).

Cell solution was prepared with human myoblasts (3×10^6 cells per myobundle) in 68.9 μL GM per bundle +8 μL of 50 U/mL thrombin (Sigma) in 0.1% BSA in PBS. In a separate vial, gelling solution (44 μL GM +40 μL Matrigel +40 μL of 20 mg/mL Fibrinogen in Tris-buffered saline and calcium chloride solution) was prepared on ice. Gelling solution was added to the cell solution, mixed thoroughly, and pipetted within the PDMS mold and onto the Cerex frame. The cell/hydrogel mixture was polymerized for 30 min at 37°C followed by incubation in GM containing 1.5 mg/mL 6-aminocaproic acid (ACA; Sigma). The next day, the frame was removed from the PDMS mold and myobundles were kept in GM containing 1.5 mg/mL ACA for 5 days during gel compaction[16] and then switched to DM containing 2 mg/mL ACA for 2 weeks.

Measurement of compaction and contractile force

Each microtissue was formed between two micropillars and compaction force was measured after 7 days of differentiation. To this end, images were taken from top to bottom (stationary part, 70 z-stacks) of the micropillars using 10 × objective of an Olympus IX81 microscope equipped with Andor™ technologies confocal system (DSD2—differential spinning disk). The deflection of micropillar heads from the stationary base was measured using ImageJ software and multiplied by the pillar's spring constant (1.2 ± 0.1 μN/μm) to calculate the force.[15]

To measure the contractile force generated by 3D tissue engineered human microtissues, external electrical stimulation was induced using a function generator (Model 4063; BK Precision, Melrose, MA) operating at 10 V to generate 200 ms electrical pulses at 1 Hz frequency for 20–30 s. These electrical parameters were optimized to yield continuous detectable contractions by the microtissues. Tissue contractions were recorded using the Zeiss Axio Observer Z1 equipped with the ORCA-ER C4742-80 digital camera. The video footage was analyzed using Tracker™ software to measure the displacement of the pillars that was multiplied by the pillar spring constant (1.2 ± 0.1 μN/μm) to calculate the force of contraction.

Measurement of intracellular calcium transients

The SkM microtissues were incubated in serum-free medium containing 5 μM calcium sensitive dye Fluo-5F, AM (ThermoFisher Scientific) for 1 h at 37°C, followed by 1 h incubation in dye-free medium. The stained microtissues were put on the stage of the Zeiss Axio Observer Z1 microscope that was equipped with an incubator chamber to maintain constant temperature at 37°C and CO_2 level at 10%. Electrical pulses were passed through the microtissues at 1 Hz, 10 V, 200 ms and videos were acquired with the ORCA-ER C4742-80 digital camera using a FITC filter and 10 × objective (Plan-APOCHROMAT). The videos were analyzed using Tracker™ software to measure changes in fluorescence signal by calculating the ratio (peak-trough)/(trough-background).

Cardiotoxin injury assay in vitro

Differentiated engineered SkM tissues were exposed to 0.2 μM cardiotoxin (CTX) (CTX; from Naja mossambica mossambica; Sigma) for 6 h on a rocker at 37°C. The injured tissues were then rinsed three times to remove the toxin and incubated in fresh DM. Immunostaining was performed on the CTX-injured tissues 6 h after CTX removal and after culture in DM for an additional 2 and 5 days.

Immunohistochemistry

Microtissues were fixed in 10% formalin for 10 min at RT and the SkM bundles were fixed in 10% formalin for 3 h at RT. The fixed microtissues or SkM bundles were

permeabilized with 0.1% (v/v) Triton X-100/PBS for 10 min at RT and blocked with blocking buffer [5% (v/v) goat serum in 0.01% (w/v) Triton X-100/PBS] at RT for 1 h. Next, samples were immunostained with antibodies against MYHC (Clone No. A4.1025, 1:500 dilution in blocking buffer; Millipore, Billerica, MA), SAA (Clone No. EP2529Y, 1:200 dilution in blocking buffer; Abcam), Ki67 (Cat No. PA5-19462, 1:200 in blocking buffer; Invitrogen), Pax7 (1:100 dilution in blocking buffer; Developmental Studies Hybridoma Bank, Iowa City, IA), and cleaved PARP (Clone No. Asp214, 1:400 dilution in blocking buffer; Cell Signaling Technology). Subsequently, the tissues were stained with Alexa Fluor 594 or 488 conjugated goat anti-mouse or goat anti-rabbit antibodies (1:200 dilution in blocking buffer; ThermoFisher Scientific) and counterstained with Hoechst 33342 nuclear dye for 5 min (1:400 dilution in PBS; ThermoFisher Scientific).

Hematoxylin and eosin stain was performed on paraffin-embedded sections (tissues were fixed in 2% paraformaldehyde) using Harris-modified hematoxylin (Sigma) and Eosin Y (Sigma) as described previously.[17] Tissue images were acquired using the Zeiss Axio Observer with LSM700 confocal module equipped with the ORCA-ER C4742-80 digital camera and analyzed using Zen Software.

Statistical analysis

Statistical analysis was performed using two-tailed unpaired Student's *t*-test or one-way ANOVA followed by Tukey's multiple comparison test using GraphPad Prism (GraphPad Software, San Diego, CA). The values were the values were considered statistically different when $p < 0.05$. Each experiment was repeated three times with at least triplicate samples in each experiment. Data were reported as mean ± standard deviation (SD) or mean ± 95% confidence interval (CI).

Results

Effects of replicative senescence on human myoblasts

To investigate the effects of cell culture time on cellular senescence of human myoblasts, we assessed some of the well-known hallmarks of aging including expression of SA-β-Gal, cellular morphology, DNA damage, cellular energetics, and histone modifications. We determined these hallmarks in cells that were cultured for different times (passages): cells cultured for <7 passages (termed young myoblast or YM); between 7 and 10 passages (termed presenescent myoblast or P-SM); or >10 passages (termed senescent myoblast or SM).

First, we determined the fraction of myoblasts versus fibroblasts over serial passaging of cells from all three donors using immunostaining for the myoblast marker (desmin) and fibroblast marker (TE7) (Supplementary Fig. S1A; 25yrF, YM: desmin+: 97.5% ± 1.7%, TE7+: 1.65% ± 1.7%, desmin–/TE7–: 0.81% ± 1.18%, SM: desmin+: 97.16% ± 3.68%, TE7+: 1.8% ± 3.27%, desmin–/TE7–: 0.96 ± 2.5%; 68yrM, YM: desmin+: 95.1% ± 2.4%, TE7+: 0.0% ± 0.0%, desmin–/TE7–: 4.91% ± 2.4%, SM: desmin+: 94.7% ± 6.7%, TE7+: 0.0% ± 0.0%, desmin –/TE7 –: 5.22% ± 6.7%; 75yrF, YM: desmin +: 93.92% ± 3.02%, TE7+: 0.66% ± 0.76%, desmin–/TE7–: 5.4% ± 3.17%, SM: desmin+: 92.7% ± 5.11%, TE7+: 0.27% ± 0.87%, desmin–/TE7–: 7.0% ± 4.92%). These results showed that the cultures were dominated by myoblasts throughout all passages.

Next, we assessed the hallmarks of aging of young, presenescent, and senescent human myoblasts. The doubling time of YM cells was ∼48 ± 1.6 h, which was significantly shorter than that of SM cells (98 ± 3.9 h) (Fig. 1A). Live/dead staining showed high cell viability regardless of passage (Supplementary Fig. S1B; cell viability, YM: 97% ± 3.74%, P-SM: 97.7% ± 4.3%, SM: 96.7% ± 4.6%, $p < 0.05$ compared with YM cells), suggesting that the reduction in cell number over time was because of reduced proliferation and not cell death. Of interest, only 15% ± 3.3% of YM cells stained positive for SA-β-Gal staining compared with 72% ± 8.5% of SM cells (Fig. 1B). Cells between passages 7 and 10 showed intermediate levels of SA-β-Gal staining (43% ± 7.2%).

Serial passaging also affected the morphology and size of the myoblast cells significantly. Specifically, the diameter and volume of P-SM and SM cells gradually increased compared with YM cells (Fig. 1C; diameter, YM: 18.65 ± 0.92 μm, P-SM: 29.14 ± 1.64 μm, SM: 36.81 ± 1.94 μm; volume, YM: 4253 ± 649 μm^3, P-SM: 18,791 ± 3025 μm^3, SM: 35,960 ± 5301 μm^3, $n = 300$ cells, $p < 0.05$ compared with YM cells). In agreement, the protein concentration in SM cells was approximately fourfold higher compared with YM cells (Fig. 1D; YM: 241 ± 100, P-SM: 512 ± 149, SM: 1,102 ± 451, $n = 5$, $p < 0.05$ compared with YM cells). Finally, P-SM and SM cells showed decreased mitotracker intensity by 1.2- and 1.3-fold, respectively, compared with YM cells, indicating compromised mitochondrial function (Fig. 1E, F; YM: 1.3 ± 0.05, P-SM: 1.2 ± 0.05, SM: 1 ± 0.04, $n = 150$ cells, $p < 0.05$ compared with YM cells).

As aging is associated with high level of DNA damage,[18] we examined the level of γH2AX using immunostaining and found that the fluorescence intensity was significantly higher in P-SM and SM cells, indicating higher levels of DNA double-strand breaks compared with YM cells (Fig. 1E, F; YM: 0.36 ± 0.02, P-SM: 0.51 ± 0.03, SM: 1 ± 0.05, $n = 150$

FIG. 1. Replicative senescence affects human myoblast proliferation, morphology, and epigenetic profile. **(A)** Population doubling time was calculated for human myoblast cells that have undergone different passage times. [YM, P-SM, and SM ($n = 3$ donors)]. **(B)** Staining for SA-β-Gal in human myoblasts and determination of the percentage of SA-β-Gal-positive cells ($n = 250$ cells) (scale bar = 100 μm). **(C)** Representative images for YM, P-SM, and SM cells (resuspended cells) to measure the diameter and volume of cells using ImageJ ($n = 300$ cells) (scale bar = 20 μm). **(D)** The total protein level of YM, P-SM, and SM cells. **(E)** Immunostaining for mitotracker and γH2AX of YM, P-SM, and SM cells (scale bar = 25 μm). **(F)** Quantification of mitotracker and γH2AX staining ($n = 150$ cells). **(G)** Immunostaining for H3K9me3 and H3K27me3 in YM, P-SM, and SM cells (scale bar = 25 μm). **(H)** Quantification of H3K9me3 ($n = 220$ cells) and H3K27me3 ($n = 220$ cells) staining. Data in bar graphs are presented as mean ± SD. Data in *dot* plots are presented as mean ± 95% confidence interval. $^{\$}$denotes $p < 0.05$ compared with all other samples. YM, young myoblast; P-SM, presenescent myoblast; SM, senescent myoblast; SA-β-Gal, senescence-associated β-galactosidase.

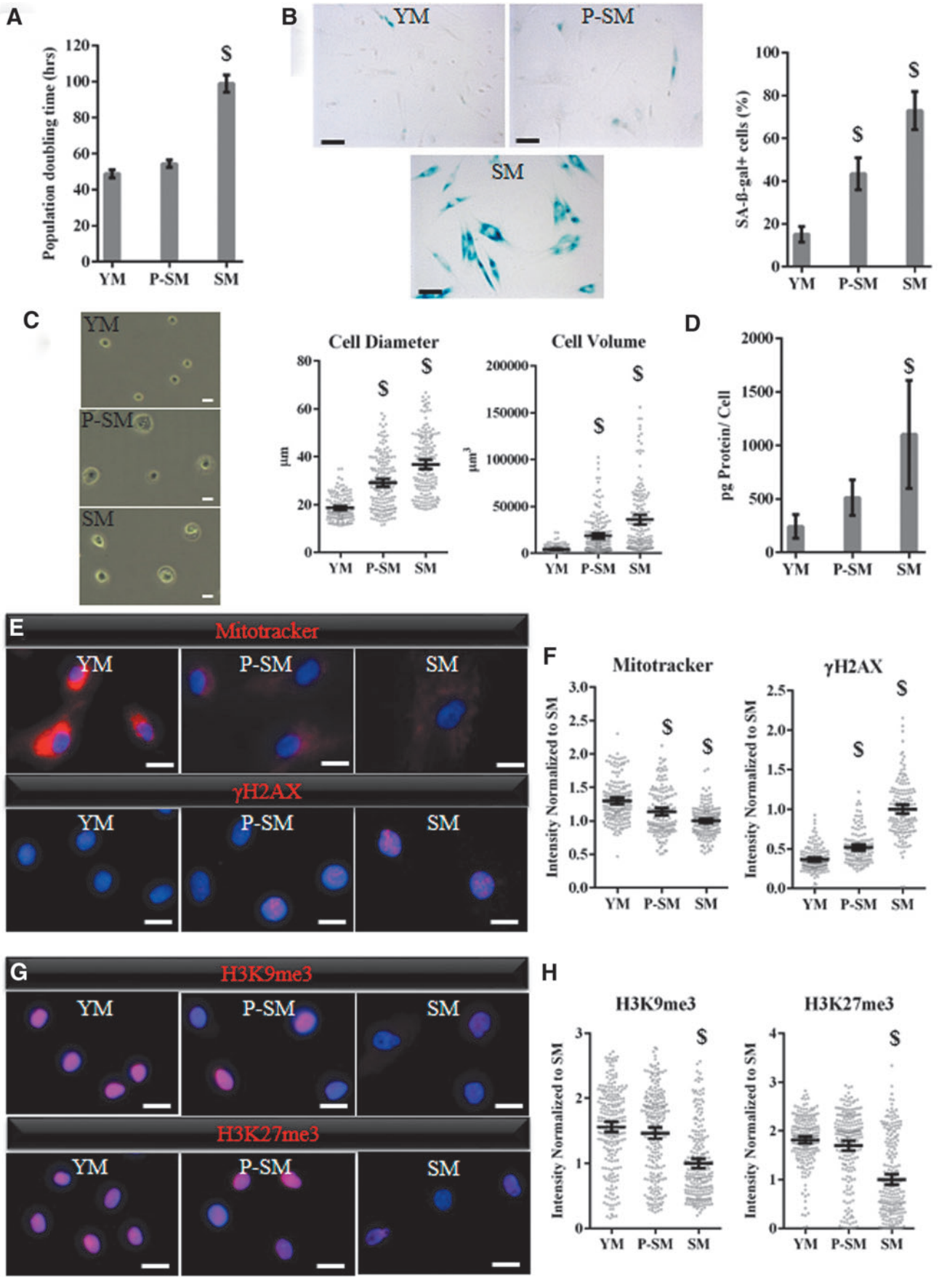
A
Population doubling time (hrs)
120
100
80
60
40
20
0
$
YM
P-SM
SM
B
YM
P-SM
SM
SA-ß-gal+ cells (%)
100
80
60
40
20
0
$
$
YM
P-SM
SM
C
YM
P-SM
SM
Cell Diameter
µm
80
60
40
20
0
$
$
YM
P-SM
SM
Cell Volume
µm³
200000
150000
100000
50000
0
$
$
YM
P-SM
SM
D
pg Protein/ Cell
2000
1500
1000
500
0
$
YM
P-SM
SM
E
Mitotracker
YM
P-SM
SM
γH2AX
YM
P-SM
SM
F
Mitotracker
Intensity Normalized to SM
3.0
2.5
2.0
1.5
1.0
0.5
0.0
$
$
YM
P-SM
SM
γH2AX
Intensity Normalized to SM
2.5
2.0
1.5
1.0
0.5
0.0
$
$
YM
P-SM
SM
G
H3K9me3
YM
P-SM
SM
H3K27me3
YM
P-SM
SM
H
H3K9me3
Intensity Normalized to SM
3
2
1
0
$
YM
P-SM
SM
H3K27me3
Intensity Normalized to SM
4
3
2
1
0
$
YM
P-SM
SM

cells, $p<0.05$ compared with YM cells). We also observed changes in the histone modification profile as evidenced by the decreased levels of H3K9me3 and H3K27me3, which are known to be affected by aging (Fig. 1G, H; H3K9me3, YM: 1.56 ± 0.08, P-SM: 1.46 ± 0.09, SM: 1 ± 0.08; H3K27me3, YM: 1.81 ± 0.07, P-SM: 1.7 ± 0.1; SM: 1 ± 0.1, $n=220$ cells, $p<0.05$ compared with YM cells).

Myogenic differentiation and compaction force of senescent human SkM cells and tissues

First, we evaluated the capability of primary human myoblasts to form myotubes in 2D culture. Myotubes were counted if they stained positive for MYHC and contained >10 nuclei. We found that the myogenic differentiation capacity of myoblasts decreased with time in culture, especially after passage 10 (Fig. 2A). The myotube diameter decreased considerably upon serial passaging (Fig. 2B; myotube diameter, YM: $101\pm6\,\mu m$, P-SM: $40\pm5\,\mu m$, SM: $23\pm2\,\mu m$, $n=5$, $p<0.05$ when each sample was compared with all others). In addition, the fusion index (FI), defined as the percentage of nuclei in myotubes, also decreased significantly (Fig. 2C; FI, YM: $63\%\pm5\%$, P-SM: $36\%\pm4\%$, SM: $14\%\pm2\%$, $n=5$, $p<0.05$ when each sample was compared with all others), as did the expression of MYHC, an important indicator of SkM function and maturation[19] (Fig. 2D; YM: 1 ± 0.17, P-SM: 0.81 ± 0.13, SM: 0.21 ± 0.03, $n=5$, $p<0.05$ when each sample was compared with all others). Of interest, there was no difference in the myotube formation capacity of myoblasts from young versus aged donors, as evidenced by the myotube diameter and FI. However, myoblasts from all donors lost their myogenic differentiation upon serial passaging (Supplementary Fig. S2A, B; myotube diameter: 25yrF, YM: $92\pm6\,\mu m$, P-SM: $40\pm4\,\mu m$, SM: $22\pm2\,\mu m$; 68yrM, YM: $94\pm8\,\mu m$, P-SM: $37\pm4\,\mu m$, SM: $25\pm1\,\mu m$; 75yrF, YM: $101\pm6\,\mu m$,

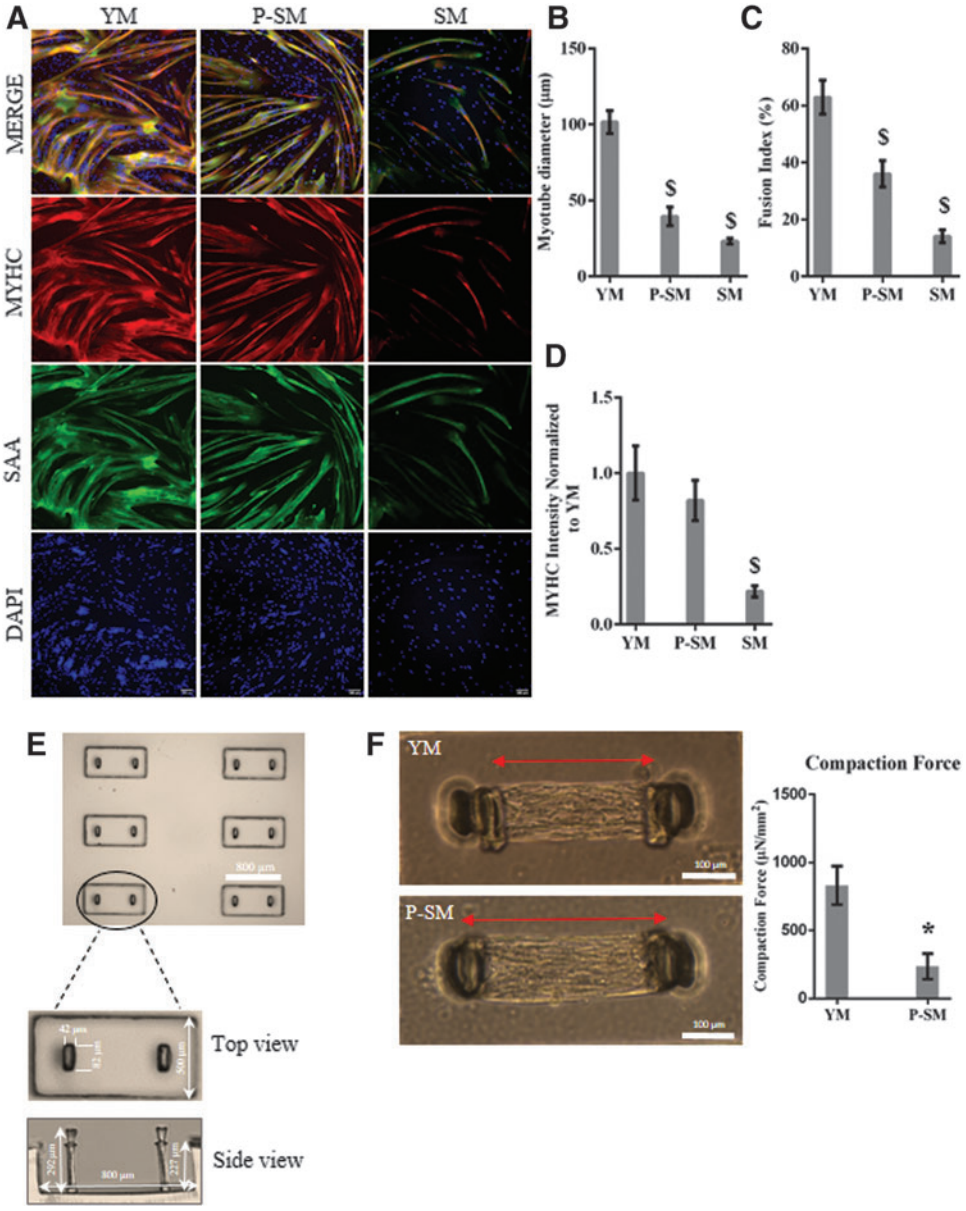

FIG. 2. Replicative senescence impairs the myogenic differentiation capacity of human myoblasts. **(A)** Immunostaining for MYHC (*red*) and SAA (*green*) nuclei (*blue*) of myotubes formed by human myoblasts at different passage number (YM, P-SM, and SM) (scale bar = 100 μm). **(B)** The average diameter of myotubes, **(C)** the fusion index (number of myonuclei/total number of nuclei × 100%), and **(D)** the average intensity of MYHC decreased significantly with time in culture. **(E)** Representative section of microarray that shows arrangement of microwells next to each other and also side view and *top* view of the microwell and micropillars. **(F)** Representative images of YM and P-SM microtissues after 7 days of differentiation and quantification of compaction force they generated ($n=9$ microtissues) (scale bar = 100 μm). Data are presented as mean ± SD. $^{*}p<0.05$ as compared with YM, $^{\$}p<0.05$ as compared with all other samples. SAA, sarcomeric alpha actinin; MYHC, myosin heavy chain.

P-SM: 40 ± 5 μm, SM: 23 ± 2 μm; FI: 25yrF, YM: 61% ± 2%, P-SM: 41% ± 7%, SM: 13% ± 2%; 68yrM, YM: 63% ± 3%, P-SM: 50% ± 7%, SM: 13% ± 2%; 75yrF, YM: 63% ± 5%, P-SM: 36% ± 54%, SM: 14% ± 2%). These results suggested that the myotube formation capacity was independent of donor age but depended strongly on replicative senescence. Because the ability of SM cells to form myotubes was diminished, we used P-SM cells to generate 3D engineered tissues, as they were still able to form myotubes although to a lesser extent than YM cells.

Using P-SM cells, we generated 3D engineered human SkM microtissue constructs to examine myotube formation and contractility. The 3D microtissues were prepared by embedding human myoblasts (5×10^5 cells/mL) in a mixture of collagen/matrigel 20% (v/v) Matrigel hydrogel[20,21] that was allowed to polymerize around a pair of flexible micropillars to generate aligned, multinucleated myofibers (Fig. 2E). After 7 days, the force of compaction was measured by the deflection of micropillars. These measurements showed that microtissues prepared with presenescent myoblasts exerted significantly lower compaction force than those containing ''younger'' cells (Fig. 2F; YM: 857 ± 120 μN/mm^2, P-SM: 244 ± 90 μN/mm^2, $n = 9$ microtissues, $p < 0.05$ compared with YM microtissues).

Contractile function of human SkM tissue

Next, we investigated the effect of cellular senescence on the contractile function of 3D engineered human microtissues. The contractions were induced by external electrical stimulation generated by a function generator as shown before,[22,23] and contractile force was measured using video microscopy (Supplementary Fig. S3A, Supplementary Videos S1, S2). The results showed that microtissues prepared with YM cells contracted in response to electrical stimulation with an average force of 42.7 ± 7 μN/mm^2, but microtissues containing P-SM cells failed to respond to electrical stimulation (0.9 ± 0.2 μN/mm^2) (Fig. 3A; $n = 9$ microtissues, $p < 0.05$, compared with YM microtissues).

Subsequently, we imaged the calcium flux in microtissues upon electrical stimulation. In agreement with force measurements, the amount of calcium in senescent microtissues was significantly lower compared with young ones (Fig. 3B, Supplementary Fig. S3B, Supplementary Videos S3, S4). Because the ATP level plays a pivotal role in providing energy for muscle contraction and calcium flux, we also measured intracellular ATP. As given in Figure 3C (intracellular ATP; YM: 26 ± 1.5 nmol/mg protein, P-SM: 21 ± 1.5 nmol/mg protein, SM: 10 ± 0.2 nmol/mg protein, $n = 3$, $p < 0.05$ compared with YM), the ATP level was significantly lower in myotubes generated with P-SM than YM cells. In agreement, senescent microtissues were less glycolytic as evidenced by significantly lower lactate levels in the culture medium, compared with the medium from YM microtissues (Fig. 3D; extracellular lactate; YM: 2101 ± 119 nmol/mg protein, P-SM: 1752 ± 130 nmol/mg protein, SM: 1004 ± 28 nmol/mg protein, $n = 3$, $p < 0.05$ compared with YM).

SkM regeneration is impaired in senescent tissues

To assess the regenerative potential of senescent SkM microtissue, we used CTX (0.2 μM) to induce injury to 3D SkM constructs. After 6 h of CTX treatment, the injury was evident by the fragmentation of muscle MYHC and SAA

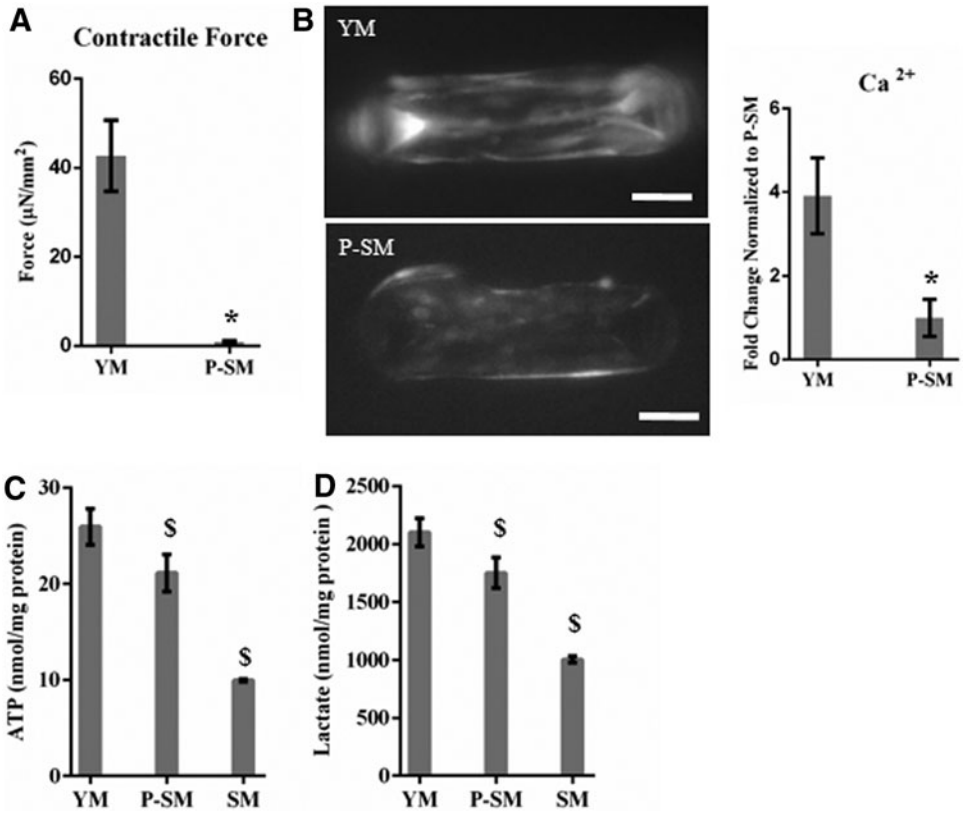

FIG. 3. Contractile and metabolic functions of human skeletal muscle tissue constructed with presenescent myoblasts decreases drastically. **(A)** Contractile force generated in response to electrical stimulation ($n = 9$ microtissues). **(B)** Representative images and quantification of intracellular calcium release in YM and P-SM microtissues in response to electrical stimulation (scale bar = 100 μm). **(C)** Intracellular ATP level was measured after 7 days of differentiation of human myoblasts. **(D)** Extracellular lactate level was measured for myotubes after 7 days of differentiation. Data are presented as mean ± SD. *$p < 0.05$ as compared with YM, $^{\$}p < 0.05$ as compared with all other samples.

fibers (Fig. 4A). In response to injury, new myotubes were observed in YM microtissues at 5 days postinjury but no recovery was observed in P-SM microtissues (Fig. 4B). To evaluate the regeneration ability of SkM microtissues, we measured the myotube diameter, length, and number of myofibers. As given in Figure 4C–E, the average myotube diameter, myotube length, and the number of myotubes per tissue were significantly impaired in P-SM microtissues (myotube diameter, YM before CTX: $14.1 \pm 1\,\mu m$, P-SM before CTX: $4.7 \pm 0.5\,\mu m$, YM 5 days after CTX: $11.7 \pm 1.6\,\mu m$, P-SM 5 days after CTX: $0.2 \pm 0.1\,\mu m$; myotube length, YM before CTX: $174 \pm 9\,\mu m$, P-SM before CTX: $104 \pm 14\,\mu m$, YM 5 days after CTX: $171 \pm 4\,\mu m$, P-SM 5 days after CTX: $2 \pm 1\,\mu m$; number of myotubes in each microtissue, YM before CTX: $5.6 \pm 0.4\,\mu m$, P-SM before CTX: $3.8 \pm 0.4\,\mu m$, YM 5 days after CTX: $5 \pm 0.8\,\mu m$, P-SM 5 days after CTX: $0.1 \pm 0.04\,\mu m$; $n = 25$ microtissues, $p < 0.05$, each sample was compared with all others).

Furthermore, we generated larger SkM tissues (2.8 cm long × 1.8 cm wide), which contain larger number of myotubes and enable better visualization of regenerated myofibers[16] (Fig. 5A). Similar to microtissues, CTX injury ($0.2\,\mu M$) for 6 h induced myotube fragmentation as evidenced by immunostaining for MYHC (Fig. 5B) and SAA (Fig. 5C; note fragmentation of Z after 6 h of CTX injury). In larger young SkM tissues, a higher number of mature myofibers were observed as evidenced by formation of Z bands before CTX (Fig. 5D). In addition, in agreement with our results with microtissues, young SkM tissues were able to regenerate myofibers 5 days after CTX injury but P-SM tissues failed to do so (Fig. 5D, immunostaining for MYHC). As a result, the average myotube diameter was significantly decreased in P-SM tissues (Fig. 5E; myotube diameter, YM before CTX: $37.18 \pm 3.4\,\mu m$, P-SM before CTX: $18.8 \pm 2\,\mu m$, YM 5 days after CTX: $31.9 \pm 4.9\,\mu m$, P-SM 5 days after CTX: $0.5 \pm 0.4\,\mu m$).

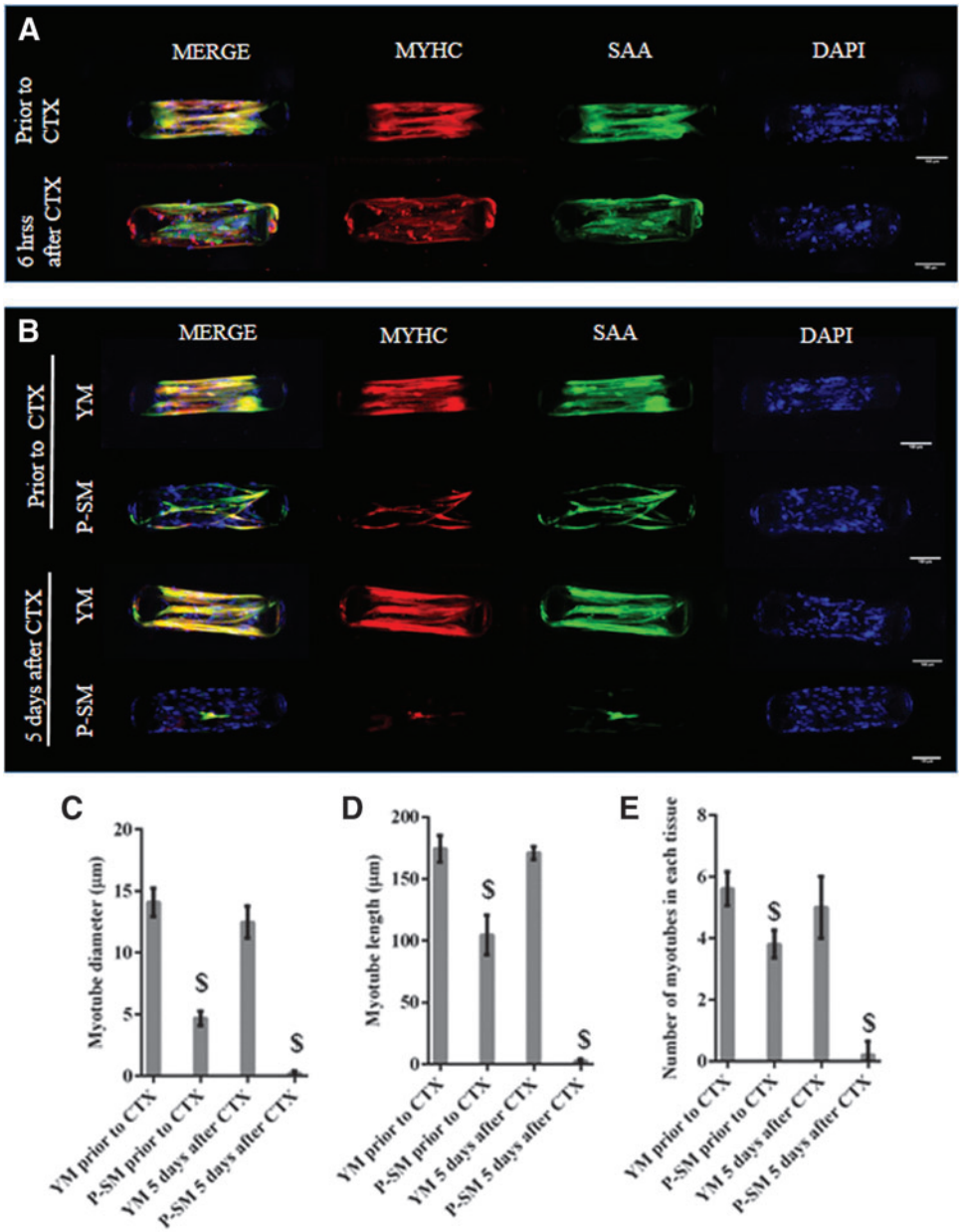

FIG. 4. Senescent bioengineered skeletal muscle tissues exhibit compromised regeneration in response to CTX injury. **(A)** Immunostaining for MYHC (*red*) and SAA (*green*) nuclei (*blue*) before and 6 h after CTX injury (scale bar = 100 μm). **(B)** Immunostaining for MYHC and SAA before and 5 days after CTX injury (scale bar = 100 μm). The **(C)** average diameter, **(D)** length, **(E)** number of myotubes in YM and P-SM tissues before or 5 days after exposure to CTX. Data are presented as mean ± SD. $^{\$}p < 0.05$ as compared with all other samples. CTX, cardiotoxin.

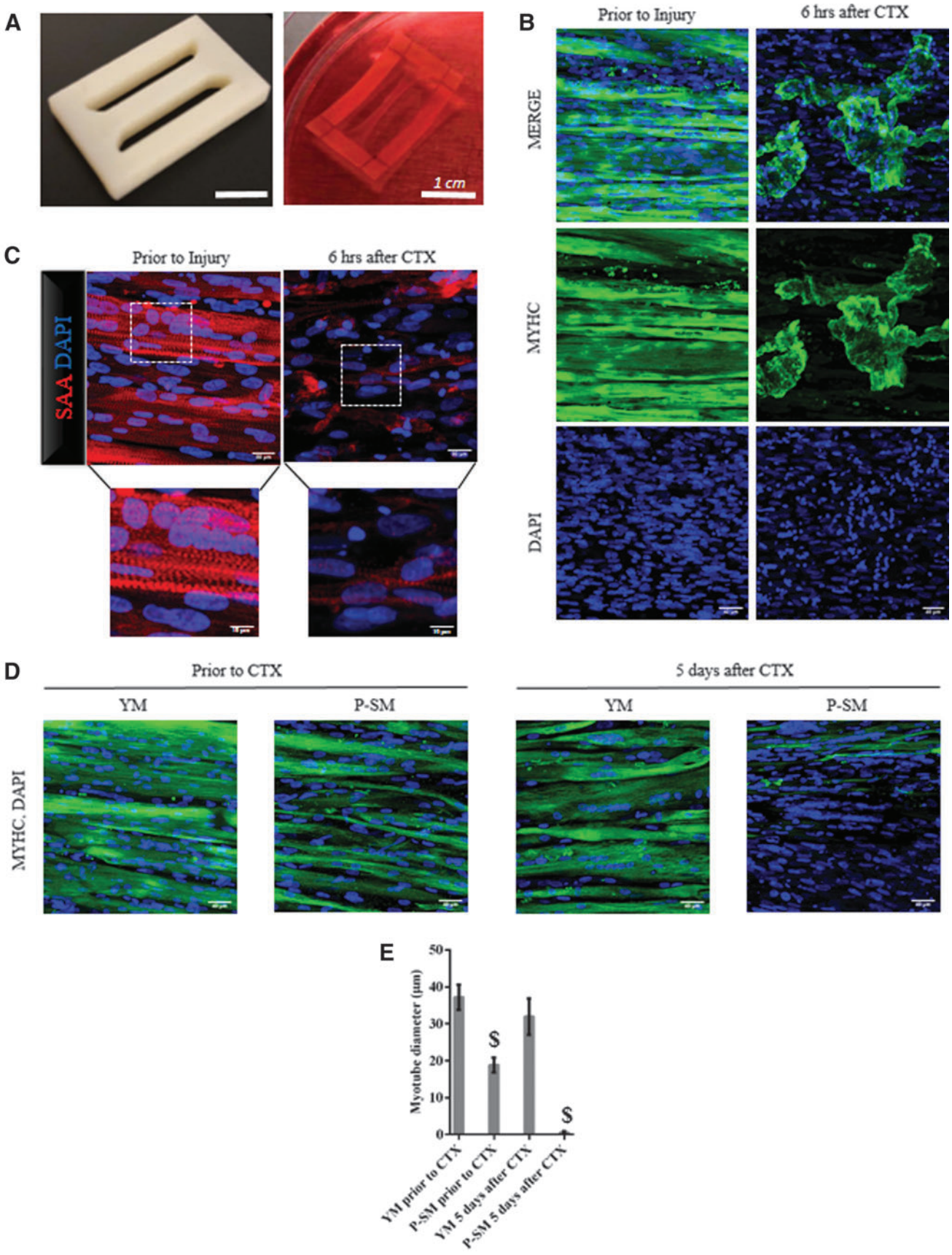

FIG. 5. Bioengineered myofibril morphology and structural organization in response to CTX injury. **(A)** PDMS mold and live image of an engineered skeletal muscle tissue (scale bar = 1 cm). **(B)** Immunostaining for MYHC before and 6 h after CTX injury (scale bar = 40 μm). **(C)** Immunostaining for SAA before and 6 h after CTX injury (main image scale bar = 20 μm; zoom in image scale bar = 10 μm). **(D)** Immunostaining for MYHC before and 5 days after CTX injury (scale bar = 40 μm). **(E)** The average diameter of myotubes in YM and P-SM tissues before and 5 days after CTX injury ($n = 6$). Data are presented as mean ± SD. $^{\$}p < 0.05$ as compared to all other samples. PDMS, polydimethylsiloxane.

Senescent tissues experience protracted apoptosis and fail to enter the cell cycle

To examine how cells responded to CTX injury, we quantified the number of satellite cells ($Pax7^+$ cells), apoptosis, and proliferation in CTX-treated tissues. Of interest, in YM tissues the percentage of $Pax7^+$ cells increased significantly at 2 days postinjury and decreased to the same level as before injury at 5 days postinjury. On the contrary, in P-SM tissues the percentage of $Pax7^+$ cells was very small and did not increase with CTX injury (Fig. 6A; YM before CTX: $9.22\% \pm 0.36\%$, YM 2 days after CTX: $18.2\% \pm 0.49\%$, YM 5 days after CTX: $11.88\% \pm 1.56\%$, $p < 0.05$, when each sample was compared with all others; P-SM before CTX: $3.3\% \pm 0.5\%$, P-SM 2 days after CTX: $5.75\% \pm 0.94\%$, P-SM 5 days after CTX: $4.9\% \pm 0.57\%$, $n = 800$ cells, $p > 0.05$).

CTX injury induced apoptosis (% Cleaved $PARP^+$ cells) in both the YM and P-SM tissues at 2 days postinjury. On day 5 postinjury, the percentage of apoptotic nuclei declined significantly in YM tissues but was sustained at high level in P-SM tissues (Fig. 6B; YM before CTX: $3.83\% \pm 0.39\%$, YM 2 days after CTX: $36.08\% \pm 2.18\%$, YM 5 days after CTX: $6.01\% \pm 0.77\%$, P-SM before CTX: $9.06\% \pm 0.66\%$, P-SM 2 days after CTX: $30.26\% \pm 1.66\%$, P-SM 5 days after CTX: $25.25\% \pm 1.4\%$, $n = 800$ cells, $p < 0.05$, when each sample was compared with all others). Of interest, proliferation (% $Ki67^+$ cells) of YM tissues increased significantly on day 2 and decreased by day 5 postinjury, in agreement with increased regeneration (Fig. 6C; YM before CTX: $1.97\% \pm 0.07\%$, YM 2 days after CTX: $17.22\% \pm 1.47\%$, YM 5 days after CTX: $0.94\% \pm 0.07\%$). However, no proliferation was observed in P-SM tissues (P-SM before CTX: $0.14\% \pm 0.11\%$, P-SM 2 days after CTX: $0.1\% \pm 0.1\%$, P-SM 5 days after CTX: $0.08\% \pm 0.08\%$, $n = 800$ cells, $p < 0.05$, each sample was compared with all others), in agreement with the lack of regeneration of $SAA^+/MYHC^+$ myofibers (Fig. 6B, C and Supplementary Fig. S4B–D). In addition, longitudinal and cross-sectional tissue sections showed that YM but not P-SM tissues contained high-density and uniformly distributed $SAA^+/MYHC^+$ myofibers (Supplementary Fig. S4B–D). Collectively, our data suggest that in young tissues apoptosis was followed by $Pax7^+$ cell activation, proliferation, and tissue regeneration, but senescent tissues exhibited protracted apoptosis and failed to activate satellite cells, initiate proliferation, and myofiber regeneration.

Discussion

Recent studies showed that replicative senescence impaired the myogenic differentiation capacity and contractile function of SkM cells.[8,9,24,25] Previous studies used the C2C12 myoblast cell line to develop a bioengineered model of SkM aging.[8,9] Although these cells display reduced myogenic differentiation capacity, they continue to proliferate and do not display any of the well-accepted hallmarks of cellular senescence. In addition, previous studies did not evaluate the contractile force generation in response to electrical stimulation or tissue regeneration in response to injury as a function of SkM tissue senescence. In this study, we utilized tissue engineered 3D human SkM constructs to assess the influence of cell senescence on the structure, function, and regenerative ability of SkM tissues. Whereas previous studies used purification strategies to obtain myoblasts devoid of contaminating fibroblasts,[26] our cell preparations from all donors contained very high levels of myoblasts (93–97.5%) and very low level of fibroblasts, even after prolonged culture times (Supplementary Fig. S1A).

In agreement with another study,[27] we observed that when myoblasts were isolated from the SkM of older adults, the nonsenescent population overtook the culture and no difference was observed between cells from young versus elderly donors, in the first few population doublings, suggesting that long-term culture was necessary to obtain cells that exhibit signs of senescence (Supplementary Fig. S2A, B). Therefore, we cultured primary human SkM cells until they reached senescence and assessed several hallmarks of aging including SA-β-Gal,[28] cellular morphology,[2] DNA damage, and histone modifications[18] as a function of time in culture. Furthermore, we examined the capacity of senescent cells to differentiate into myotubes. Our findings demonstrated that myoblasts begin to show signs of senescence starting at passage 7, for example, loss of myotube formation potential as evidenced by atrophied myotubes of decreased diameter. Beyond passage 10, myoblasts lost their capacity to form myotubes and express actinin and MYHC. These results suggest that some tissue functions, such as myotube formation or force generation capacity, may be lost earlier in the continuum of senescence. Consequently, to develop 3D tissue engineered senescent SkM constructs, we chose cells between passage 7 and 10, which showed signs of senescence but had not lost their ability to form myotubes (constructs with cells $7 < p < 10$ cells).

As expected, young microtissues constructed from YM cells resulted in functional myotubes that contracted in response to electrical stimulation. In contrast, the contractile force that was generated by senescent microtissues was $\sim$35-fold lower compared with that of young ones. Similarly, senescent microtissues exhibited significantly reduced Ca^{2+} flux compared with young microtissues. These results showed that the atrophied senescent myotubes exhibited significantly compromised function, prompting us to examine the cellular energetics and the regenerative capacity of aged SkM tissue constructs.

Indeed, senescent myotubes exhibited decreased ATP synthesis in agreement with clinical data showing that the muscles of the elderly people exhibit lower levels of ATP.[29] At the same time, senescent myotubes showed decreased lactate production, suggesting reduced rate of glycolysis, the primary pathway for energy production in SkM.[30,31] Therefore, reduced ATP and lactate levels in aged myotubes may explain the decreased contractile function and impaired regenerative capacity of senescent SkM tissues.

SkM has the ability to regenerate and heal itself, primarily through activation of a quiescent population of myogenic cells in response to injury. However, aging is associated with a significant decline in the number of myogenic progenitors leading to significant loss in regenerative capacity.[4,32,33] Here we subjected the 3D bioengineered SkM tissues to injury, to examine the effect of cellular senescence on tissue regeneration. In agreement with studies in animals, young tissues exhibited a remarkable ability to repair the CTX-induced injury within 5 days,[34] whereas senescent

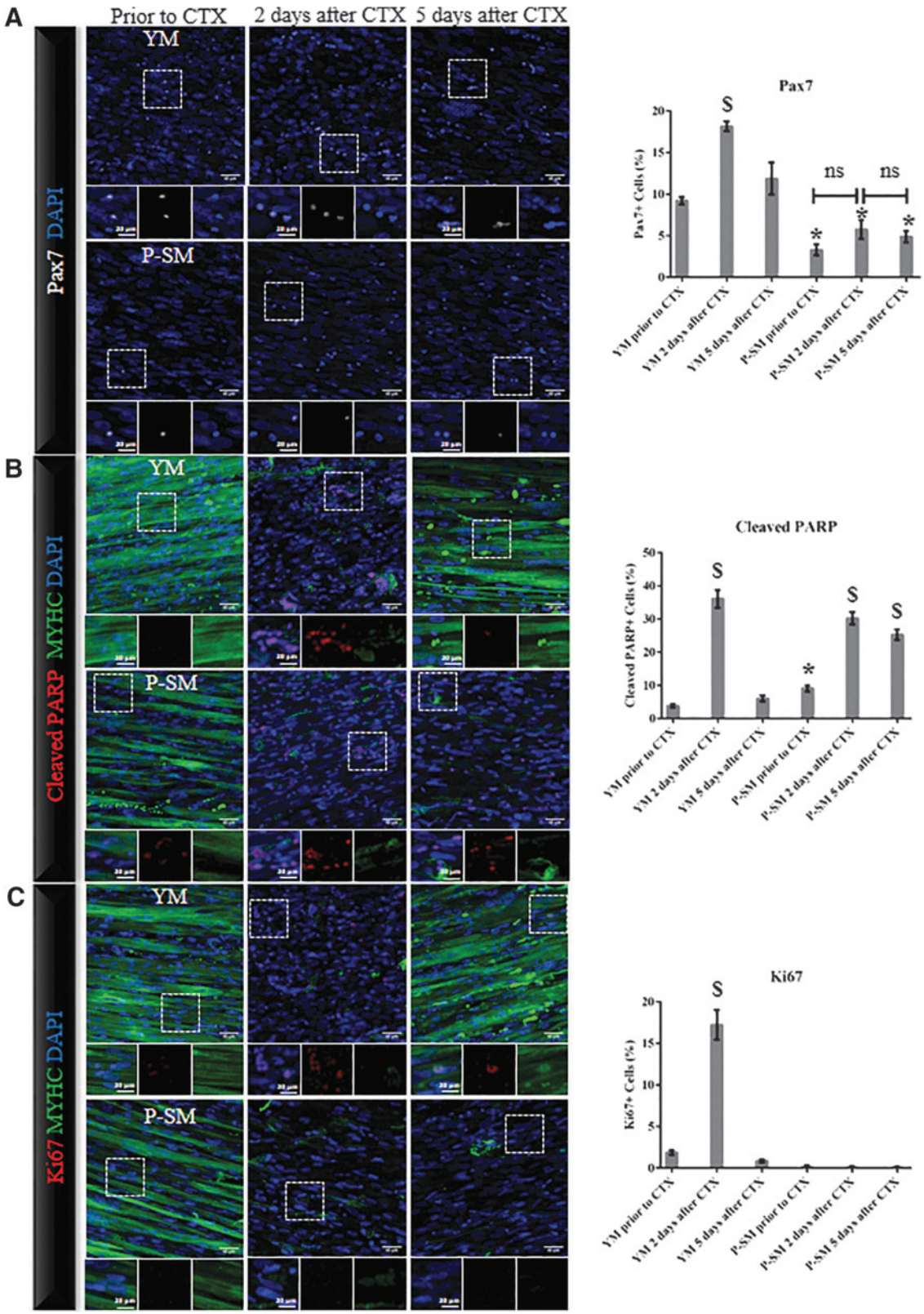

FIG. 6. Regenerative response of engineered muscle to CTX injury. **(A)** Immunostaining for Pax7 before or 2 and 5 days after CTX injury. (scale bar = 40 μm) and quantification of the percentage of $Pax7^+$ cells ($n = 800$ cells). **(B)** Immunostaining for MYHC and cleaved PARP before or 2 and 5 days after CTX injury (scale bar = 40 μm) and quantification of the percentage of cleaved $PARP^+$ cells ($n = 800$ cells). **(C)** Immunostaining for MYHC and Ki67 before or 2 and 5 days after CTX injury (scale bar = 40 μm) and quantification of the percentage of $Ki67^+$ cells ($n = 800$ cells) **(A-C)** For zoom in images below the main image, scale bar = 20 μm. Data are presented as mean ± SD. $^*p < 0.05$ compared with YM before CTX injury, $^{\$}p < 0.05$ compared with all other samples. ns, not significant.

tissues failed to do so.[35,36] Of interest, although both young and senescent tissues contained apoptotic cells, only young tissues were immunopositive for Pax7 and Ki67, indicating activation of Pax7 and initiation of proliferation to replace the injured cells. In contrast, senescent tissues failed to activate Pax7 expression and initiate proliferation but exhibited increased apoptosis, as evidenced by higher cleaved PARP levels. This result is in agreement with cell transplantation studies in Pax7 knockout mice demonstrating the requirement of $Pax7^+$ cells for injury-induced muscle regeneration.[37] Taken together, our data suggested that senescent SkM tissues failed to regenerate, possibly as a result of protracted apoptosis, depletion of satellite cells, and failure to initiate proliferation and subsequent fusion to form *de novo* myofibers. It would be interesting to use this system to test chemical and biological compounds such as hormones,[38,39] antioxidants, or mechanical forces, alone or in combination, to examine whether they can improve or even reverse the regeneration capacity of human senescent myofibers. In summary, our findings indicate that similar to aged organisms, senescent 3D SkM constructs exhibited impaired ability to regenerate in response to injury and therefore, they may provide a model to study senescence, wound healing, and muscle wasting disorders, and also provide a platform for pharmacological testing in a 3D setting that better mimics the *in vivo* behavior of SkM tissue.

Conclusion

In this work, we present a senescent model of bioengineered SkM that can be used to investigate senescence, metabolic or genetic diseases that inflict SkM, and to test various strategies including novel small molecules that restore muscle function and promote regeneration. Although 2D cultures are limited in their ability to simulate the contractile response of SkM to various stimuli, the 3D constructs enable organization of contractile units including myosin and actin filaments, thereby providing a platform for the quantitative assessment of muscle myotubes in response to injury, genetic or metabolic disorders or pharmacological testing.

Authors' Contributions

Experiments were planned and designed by Nika Rajabian and Stelios T. Andreadis. Experimental data were generated and collected by Nika Rajabian, Mohammadnabi Asmani, Aref Shahini, Kalyan Vydiam, Debanik Choudhury, Thy Nguyen, Izuagie Ikhapoh. Data analysis and interpretation were done by Nika Rajabian, Aref Shahini, Stelios T. Andreadis. Writing and critical revisions of the manuscript were performed by Nika Rajabian, Pedro Lei, Stelios T. Andreadis.

Disclosure Statement

No competing financial interests exist.

Funding Information

This study was supported by a grant from the National Institute on Aging (R01 AG052387) and National Heart Blood and Lung Institute (5R01 HL086582) to S.T.A.

Supplementary Material

Supplementary Figure S1
Supplementary Figure S2
Supplementary Figure S3
Supplementary Figure S4
Supplementary Video S1
Supplementary Video S2
Supplementary Video S3
Supplementary Video S4

References

1. David, W.R. and Ian, R.L. The impact of old age on skeletal muscle energetics: supply and demand. Curr Aging Sci **4,** 234, 2011.
2. Nehlin, J.O., Just, M., Rustan, A.C., and Gaster, M. Human myotubes from myoblast cultures undergoing senescence exhibit defects in glucose and lipid metabolism. Biogerontology **12,** 349, 2011.
3. Rosenberg, I.H. Sarcopenia: origins and clinical relevance. J Nutr **127,** 990S, 1997.
4. Carosio, S., Berardinelli, M.G., Aucello, M., and Musarò, A. Impact of ageing on muscle cell regeneration. Ageing Res Rev **10,** 35, 2011.
5. Janssen, I., Shepard, D.S., Katzmarzyk, P.T., and Roubenoff, R. The healthcare costs of Sarcopenia in the United States. J Am Geriatr Soc **52,** 80, 2004.
6. Tedesco, F.S., Dellavalle, A., Diaz-Manera, J., Messina, G., and Cossu, G. Repairing skeletal muscle: regenerative potential of skeletal muscle stem cells. J Clin Invest **120,** 11, 2010.
7. Miljkovic, N., Lim, J.-Y., Miljkovic, I., and Frontera, W.R. Aging of Skeletal Muscle Fibers. Ann Rehabil Med **39,** 155, 2015.
8. Sharples, A.P., Player, D.J., Martin, N.R.W., Mudera, V., Stewart, C.E., and Lewis, M.P. Modelling in vivo skeletal muscle ageing in vitro using three-dimensional bioengineered constructs. Aging Cell **11,** 986, 2012.
9. Shahini, A., Choudhury, D., Asmani, M., Zhao, R., Lei, P., and Andreadis, S.T. NANOG restores the impaired myogenic differentiation potential of skeletal myoblasts after multiple population doublings. Stem Cell Res **26,** 55, 2018.
10. Toral-Ojeda, I., Aldanondo, G., Lasa-Elgarresta, J., et al. A Novel Functional In Vitro Model that Recapitulates Human Muscle Disorders. Tokyo, Japan: Tokyo Institute of Technology, 2018.
11. Sammons, M.A., Antons, A.K., Bendjennat, M., Udd, B., Krahe, R., and Link, A.J. ZNF9 activation of IRES-mediated translation of the human ODC mRNA is decreased in myotonic dystrophy type 2. PLoS One **5,** e9301, 2010.
12. Agley, C.C., Rowlerson, A.M., Velloso, C.P., Lazarus, N.L., and Harridge, S.D.R. Isolation and quantitative immunocytochemical characterization of primary myogenic cells and fibroblasts from human skeletal muscle. JoVE **95**, e52049, 2015.
13. Bradford, M.M., A rapid and sensitive method for the quantitation of microgram quantities of protein utilizing the principle of protein-dye binding. Anal Biochem **72,** 248, 1976.
14. Debacq-Chainiaux, F., Erusalimsky, J.D., Campisi, J., and Toussaint, O. Protocols to detect senescence-associated beta-galactosidase (SA-βgal) activity, a biomarker of se-

nescent cells in culture and in vivo. Nat Protoc **4,** 1798, 2009.
15. Legant, W.R., Pathak, A., Yang, M.T., Deshpande, V.S., McMeeking, R.M., and Chen, C.S. Microfabricated tissue gauges to measure and manipulate forces from 3D microtissues. Proc Natl Acad Sci U S A **106,** 10097, 2009.
16. Madden, L., Juhas, M., Kraus, W.E., Truskey, G.A., and Bursac, N. Bioengineered human myobundles mimic clinical responses of skeletal muscle to drugs. eLife **4,** e04885, 2015.
17. Shahini, A., Vydiam, K., Choudhury, D., et al. Efficient and high yield isolation of myoblasts from skeletal muscle. Stem Cell Res **30,** 122, 2018.
18. López-Otín, C., Blasco, M.A., Partridge, L., Serrano, M., and Kroemer, G. The hallmarks of aging. Cell **153,** 1194, 2013.
19. Lowey, S., Waller, G.S., and Trybus, K.M. Function of skeletal muscle myosin heavy and light chain isoforms by an in vitro motility assay. J Biol Chem **268,** 20414, 1993.
20. Sakar, M.S., Neal, D., Boudou, T., et al. Formation and optogenetic control of engineered 3D skeletal muscle bioactuators. Lab Chip **12,** 4976, 2012.
21. Shahini, A., Mistriotis, P., Asmani, M., Zhao, R., and Andreadis, S.T. NANOG restores contractility of mesenchymal stem cell-based senescent microtissues. Tissue Eng Part A **23,** 535, 2017.
22. Bottinelli, R. and Reggiani, C. Human skeletal muscle fibres: molecular and functional diversity. Prog Biophys Mol Biol **73,** 195, 2000.
23. Fuglevand, A.J., Macefield, V.G., and Bigland-Ritchie, B. Force-frequency and fatigue properties of motor units in muscles that control digits of the human hand. J Neurophysiol **81,** 1718, 1999.
24. Bigot, A., Jacquemin, V., Chainiaux, F., et al. Replicative aging down-regulates the myogenic regulatory factors in human myoblasts. Biol Cell **100,** 189, 2008.
25. Sharples, A.P., Al-Shanti, N., Lewis, M.P., and Stewart, C.E. Reduction of myoblast differentiation following multiple population doublings in mouse C2C12 cells: A model to investigate ageing? J Cell Biochem **112,** 3773, 2011.
26. Martin, N.R.W., Passey, S.L., Player, D.J., et al. Factors affecting the structure and maturation of human tissue engineered skeletal muscle. Biomaterials **34,** 5759, 2013.
27. Alsharidah, M., Lazarus, N.R., George, T.E., Agley, C.C., Velloso, C.P., and Harridge, S.D.R. Primary human muscle precursor cells obtained from young and old donors produce similar proliferative, differentiation and senescent profiles in culture. Aging Cell **12,** 333, 2013.
28. Lee, B.Y., Han, J.A., Im, J.S., et al. Senescence-associated β-galactosidase is lysosomal β-galactosidase. Aging Cell **5,** 187, 2006.
29. Johnson, M.L., Robinson, M.M., and Nair, K.S. Skeletal muscle aging and the mitochondrion. Trends Endocrinol Metab **24,** 247, 2013.
30. Baker, J.S., McCormick, M.C., and Robergs, R.A. Interaction among Skeletal Muscle Metabolic Energy Systems during Intense Exercise. Journal of nutrition and metabolism **2010,** 905612, 2010.
31. Papa, S., Choy, P.M., and Bubici, C. The ERK and JNK pathways in the regulation of metabolic reprogramming. Oncogene **38,** 2223, 2019.
32. Shefer, G., Van de Mark, D.P., Richardson, J.B., and Yablonka-Reuveni, Z. Satellite-cell pool size does matter: defining the myogenic potency of aging skeletal muscle. Dev Biol **294,** 50, 2006.
33. Day, K., Shefer, G., Shearer, A., and Yablonka-Reuveni, Z. The depletion of skeletal muscle satellite cells with age is concomitant with reduced capacity of single progenitors to produce reserve progeny. Dev Biol **340,** 330, 2010.
34. Yin, H., Price, F., and Rudnicki, M.A. Satellite cells and the muscle stem cell niche. Physiol Rev **93,** 23, 2013.
35. Mouisel, E., Vignaud, A., Hourdé, C., Butler-Browne, G., and Ferry, A. Muscle weakness and atrophy are associated with decreased regenerative capacity and changes in mTOR signaling in skeletal muscles of venerable (18–24-month-old) dystrophic mdx mice. Muscle Nerve **41,** 809, 2010.
36. Jang, Y.C., Sinha, M., Cerletti, M., Dall'Osso, C., and Wagers, A.J. Skeletal muscle stem cells: effects of aging and metabolism on muscle regenerative function. Cold Spring Harb Symp Quant Biol **76,** 101, 2011.
37. Lepper, C., Partridge, T.A., and Fan, C.-M. An absolute requirement for Pax7-positive satellite cells in acute injury-induced skeletal muscle regeneration. Development **138,** 3639, 2011.
38. Deane, C.S., Hughes, D.C., Sculthorpe, N., Lewis, M.P., Stewart, C.E., and Sharples, A.P. Impaired hypertrophy in myoblasts is improved with testosterone administration. J Steroid Biochem Mol Biol **138,** 152, 2013.
39. Hughes, D.C., Stewart, C.E., Sculthorpe, N., et al. Testosterone enables growth and hypertrophy in fusion impaired myoblasts that display myotube atrophy: deciphering the role of androgen and IGF-I receptors. Biogerontology **17,** 619, 2016.

Address correspondence to:
Stelios Andreadis, PhD
Department of Chemical and Biological Engineering
University at Buffalo
The State University of New York
Bioengineering Laboratory
908 Furnas Hall
Buffalo, NY 14260-4200
USA

E-mail: sandread@buffalo.edu

Received: January 7, 2020
Accepted: April 28, 2020
Online Publication Date: June 16, 2020